Angular momentum dependence of the nuclear level-density parameter around $Z \sim 50$

Y. K. Gupta,* Bency John, D. C. Biswas, B. K. Nayak, A. Saxena, and R. K. Choudhury
Nuclear Physics Division, Bhabha Atomic Research Centre, Mumbai 400 085, India
(Received 8 April 2008; published 26 November 2008)

α-particle evaporation spectra and γ-ray multiplicities were measured for various target-projectile systems corresponding to residual nuclei in the range of $Z_R = 48$–55 and with excitation energy in the range of 30–40 MeV. The high-energy part of the evaporation spectra were analyzed using the statistical model code PACE2 to derive values of the inverse level-density parameter (K). The K values were found to be in the range of 9.0–10.5 for all systems. Angular momentum dependence of the inverse level-density parameter was investigated using the γ-ray multiplicity data. It is seen that there are strong variations in K as a function of angular momentum for many systems. Present results provide important input information for a systematic understanding of the statistical properties of nuclei at moderate excitation energies and angular momenta.

DOI: 10.1103/PhysRevC.78.054609 PACS number(s): 21.10.Ma, 21.10.Re, 24.60.Dr, 27.60.+j

I. INTRODUCTION

The nuclear level density contains important information on the microscopic features and statistical aspects of an excited nucleus and is a key ingredient in the calculation of reaction cross sections using the framework of the Hauser-Feshbach (HF) theory of compound nuclear reactions. Practical applications of HF theory require global knowledge of nuclear level densities and these are best served by a phenomenological level-density function, known in the literature as the back-shifted Fermi-gas (BSFG) formula [1]. There are two fundamental parameters in the BSFG formula: the level-density parameter a and the spin cut-off parameter σ^2. There have been many attempts (e.g., Refs. [2–10]) to refine the knowledge of these parameters, as there could be large uncertainties in reaction cross-section calculations due to variations in these parameters. Most of the earlier attempts have been concentrated on low excitation energy and the low-spin region because the relevant, accurate, and extensive experimental data (from s-wave neutron resonance spacing and density of low-lying discrete states in the excitation energy region below approximately 8 MeV) are available in this region. The inverse level-density parameter $K(K = A/a, A = \text{mass number})$ obtained from these studies shows a considerable deviation from a constant value, implying presence of unaccounted microscopic features in the Fermi gas assumption. These features have been normally identified with the influence of shell effects prevailing at low excitation energies, and many refinements [2,3] have been carried out for the level-density parameter based on these systematics. The low-angular-momentum (J) states in s-wave neutron resonance absorption ($J = I \pm 1/2$, where I is the spin of the target nucleus in its ground state) do not allow determination of σ^2 over a range of angular momenta. In the Fermi-gas model, the spin cut-off parameter is determined according to $\sigma^2 = \langle m^2 \rangle gt = \Im t/\hbar^2$, where $\langle m^2 \rangle$ is the average of the squares of the single-particle spin projections, t is thermodynamic temperature, $\Im$ is the nuclear moment of inertia, and g is single-particle level density at the Fermi energy, ϵ_F. In the absence of reliable experimental information on angular-momentum distribution of levels over a wide range of J to validate σ^2, the Fermi-gas model values are used as such in reaction cross-section calculations.

A sustained effort for describing nuclear level density using microscopic theories is underway in parallel to the developments in phenomenological studies. The phenomenological descriptions mainly ignore the residual interactions of nucleons except for pairing that is partly taken into account by the back-shift energy. In recent times, advances taking place in microscopic calculations also emphasize the spin distribution of levels. The shell-model Monte Carlo method has been demonstrated for the calculation of the spin distribution of nuclear levels below the neutron separation energy [4]. Spin distribution of nuclear levels has been calculated [5] microscopically using random-phase and static-path approximations (RPA-SPA) without the assumption of individual random spin vectors. Also, the spin cut-off parameter was calculated [6] at neutron binding energies over a large range of nuclear masses using the BCS theory. The work presented in Ref. [6] has been accomplished using realistic values of single-particle energies ϵ_k and their corresponding magnetic quantum number m_k. It was found that the values of this parameter do not increase smoothly with A as expected from the Fermi-gas model. Instead, the values showed structures that are significantly different compared to the rigid-body values, reflecting the angular momentum of the shell-model orbitals near ϵ_F. Examination of the single-particle level scheme (ϵ_k, m_k) for nuclei in the mass region where the differences between rigid-body and BCS values are large indicated that the orbitals with large angular momenta are responsible for this observation.

Due to these recent advances in the theory, it is necessary to carry out experimental investigations of nuclear level density at various excitation energies and angular momentum domains. In the present work, we have developed a method for extracting nuclear level densities as a function of angular momentum. Using this method we have obtained results for the inverse level-density parameter as a function of angular momentum for a number of nuclei in $Z \sim 50$ shell region at an excitation energy around 30 to 40 MeV. We have used heavy-ion

*ykgupta@barc.gov.in

TABLE I. The reactions studied in the present work and relevant experimental parameters.

Index	Reaction	Z_R	α	$E_{\text{laboratory}}$ (MeV)	$E_{\text{ex}}^{\text{CN}}$ (MeV)	l_{graz} ($\hbar$)	K[a] (MeV)	ν_α Expt. (Cal.)[a]
a	$^{19}\text{F} + ^{93}\text{Nb}$	48	0.6607	73.5	60.0	29.5	9.6 ± 0.1	0.27(0.20)
b	$^{24}\text{Mg} + ^{89}\text{Y}$	49	0.5752	100.5	60.6	38.9	9.0 ± 0.1	0.72(0.52)
c	$^{27}\text{Al} + ^{89}\text{Y}$	50	0.5345	106.0	60.4	38.9	8.8 ± 0.1	0.57(0.42)
d	$^{24}\text{Mg} + ^{93}\text{Nb}$	51	0.5897	103.3	60.3	39.7	9.4 ± 0.2	0.72(0.78)
e	$^{11}\text{B} + ^{115}\text{In}$	52	0.8254	58.0	61.0	30.1	10.3 ± 0.3	0.06(0.10)
f	$^{12}\text{C} + ^{115}\text{In}$	53	0.8110	71.0	61.0	34.7	10.5 ± 0.3	0.07(0.17)
g	$^{16}\text{O} + ^{115}\text{In}$	55	0.7557	80.0	59.2	35.6	9.5 ± 0.3	0.18(0.19)

[a]For gross spectra.

fusion reactions to populate the excited, rotating nuclei and characterized their level density as a function of angular momentum by measuring the α-particle evaporation spectra in coincidence with γ-ray multiplicity. The reactions were selected to populate residual nuclei in $Z \sim 50$ shell region after α-particle evaporation. The relevant parameters of the fusion reactions are given in Table I. The target-projectile systems selected in the present work correspond to a range of entrance-channel mass asymmetry, $\alpha = (A_T - A_P)/(A_T + A_P)$. An analysis of the reactions based on Businaro-Gallone critical mass asymmetry (α_{BG}) for various ℓ-partial waves (Sec. IV) reveals that all these reactions will undergo normal compound nuclear formation without a dinuclear complex formation ($\alpha > \alpha_{\text{BG}}$). The bombarding energies were chosen such that all the compound nuclei are formed with a 60-MeV excitation energy. The spin-dependent level density makes its most noticeable change in the slope of the high-energy tail of the evaporation spectra. This slope is least influenced by the barrier transmission factors. For the present study, we focus on the high-energy tail of the α-particle spectra, although the spectra were measured over a wider range of energies. By tagging the α-particle energy spectra with the γ-ray-multiplicity fold signal defined in Sec. II, the angular-momentum dependence of the level-density parameter was derived. In the data analysis, each fold value was converted to a corresponding average angular momentum following a procedure that utilizes decay simulation and detector efficiency factors. The shape of the fold-gated α-particle energy spectra was analyzed at energies well above the evaporation barrier. We obtain K values as a function of angular momentum for the residual nuclei by fitting the experimental fold-gated spectra with simulated spectra using the code PACE2 [11].

Selection of the high-emission-energy region for the analysis leads to a specific excitation energy range in the residual nuclei for which the results obtained are valid [12]. In the present work, this range is from 30 to 40 MeV. Because the multiplicity of α particles and other charged particles are less than unity in the present reactions, it can be safely assumed that α-particle emission leaves residual nuclei with $Z_R = Z_{\text{CN}} - 2$ and our results are valid for these $Z(Z_R)$ values.

The present article is organized in the following way. The experimental setup is described in Sec. II. Section III contains the data analysis method. The results and discussion are presented in Sec. IV. Finally, the summary is presented in Sec. V.

II. EXPERIMENTAL DETAILS

The experiments were performed using heavy-ion beams from the BARC-TIFR 14-MV Pelletron accelerator facility at Mumbai. A compact scattering chamber and a γ-ray-multiplicity setup consisting of 14 BGO detectors were used for the measurements. Self-supporting thin metallic foils of the targets having thickness in the range of 500–750 μg/cm^2, were mounted on the target ladder and placed at right angle to the beam. α particles emitted in the reactions were detected by two collimated silicon surface barrier ΔE-E (25 μm-2 mm) detector telescopes mounted in the median (reaction) plane at back angles. A number of systems were studied as listed in Table I and the measurements were carried out in two separate experiments. In the first set of experiments, reactions (a) to (d) were studied and in the second set, reactions (e) to (g) were studied. The telescopes were of equal solid angle of 5.94 msr and were kept at $\theta_{\text{lab}} = 116^\circ$ and 125° for the first set and at $\theta_{\text{lab}} = 125^\circ$ and 153° for the second set. Another surface-barrier detector having a solid angle of 0.20 msr was mounted at $\theta_{\text{lab}} = 16^\circ$ for normalization with Rutherford scattering events. The telescopes were energy calibrated using α particles from a ^{228,229}Th source and with ^{7}Li ions elastically scattered off a thin ^{197}Au (^{209}Bi in the second set) target. Calibration energies ranged from 6.3 to 30 MeV. Energy loss of the incident ^{7}Li ions in the target was taken into account in determining the energy calibration. Similarly, energy loss of emitted α particles through the target foil was taken into account in determining their final energy. Table I gives other experimental parameters such as charge Z_R of residual nuclei after α-particle evaporation, entrance-channel mass asymmetry α, bombarding energy E_{lab}, compound nucleus excitation energy $E_{\text{ex}}^{\text{CN}}$, and grazing angular momentum values l_{graz} for the systems studied in the present work.

Fourteen BGO detectors were mounted on top and bottom of the reaction plane in two close-packed groups of seven each. The two groups were placed at a distance of $\sim$2.5 cm on either side of the reaction plane. The middle detector in each group was pulled out to nearly equalize the efficiency of all the detectors. The energy threshold of the BGO detectors was adjusted to be 150-keV (100 keV for the second set) γ-ray energy. The efficiency of the setup was measured for 662-keV γ rays emitted from a ^{137}Cs source of known strength placed at the target position and the total efficiency was determined to be 51% (55% in the second set). The pulse heights from the ΔE-E detector telescopes and the BGO timing outputs were recorded

in list-mode using a multiparameter data acquisition system. The fold-gated α-particle energy spectra were projected out from the list-mode data after putting suitable two-dimensional gate on the α-particle band and on the γ-ray-multiplicity fold number. Fold is defined as the number of BGO detectors firing simultaneously in an event.

Light mass impurities such as carbon and oxygen that are present in the targets created low-energy tails in the energy spectra for two of the light projectiles (^{11}B and ^{12}C). α particles originating from the reactions with impurity elements appeared in the spectra at low energies, particularly for the low multiplicity folds. This low-energy component was treated as a background and was removed by following a least-squares fit procedure as discussed below. As the projectile mass increased from ^{11}B, the background became less severe. For ^{16}O and heavier ions, there was no appreciable interference of impurity events even for low folds. Every fold-gated spectrum was examined for the presence of this background. It was observed that the background falls off exponentially with energy. This dependence of the background on the fold as well as the α-particle energy is illustrated in a gross manner in two-dimensional plots in Fig. 1 for all the systems. Further analysis was carried out only for fold-1 and above, where the background is seen to be negligible.

In the fits to remove the background, an initial estimation of the exponential fall of the background was made in the energy region of 5 to 10 MeV where the low energy tail is dominant, using a function $N_1 \exp(-E/T_B)$, where N_1 is a normalization constant and T_B is a slope parameter. The values of N_1 and T_B thus obtained were used as initial values in the composite function

$$\text{Yield} = N_1 \exp(-E/T_B) + N_2 E \frac{\exp(-E/S_1)}{1+\exp\left(\frac{E_b-E}{S_2}\right)}, \quad (1)$$

where the second term in the right-hand side with a normalization factor N_2, emission barrier energy factor E_b, and slope factors S_1 and S_2 models the shape of the α-particle spectrum in laboratory system. By fitting the spectrum using Eq. (1) in the energy interval of 5 MeV to 30 MeV, values of N_1 and T_B were optimized for the whole energy interval. As a typical case for background subtraction, the energy spectra for folds 1 to 3 from ^{11}B + ^{115}In are shown in the top panels of Fig. 2. The spectra before and after background subtraction are shown using filled circles and open squares, respectively. The dotted line in the figure is the low-energy back ground part obtained using the optimized parameters N_1 and T_B in the function $N_1 \exp(-E/T_B)$. It was observed that for the fold 1 spectrum the estimated background was less than 0.3% at 15 MeV of α-particle energy and it exponentially reduces at higher energies. The influence of background in determining the slope of the high-energy tail (>15 MeV) is negligible. For folds 2 and 3 the influence of the background is further strongly reduced [Figs. 2(b) and 2(c)] and for still higher folds [fold 4 to 6, Figs. 2(d)–2(f)] the data are essentially free of background above an energy of 15 MeV in the laboratory system. The laboratory spectra obtained after background subtraction were transformed to compound nucleus center-of-mass (c.m.) system using the standard Jacobian [13]. In the center-of-mass system, the spectra measured at both angles overlapped very well for each fold, indicating that the spectra originated in the evaporation process. The average spectra obtained from the data at two angles were compared with PACE2 calculations to derive the level-density parameter.

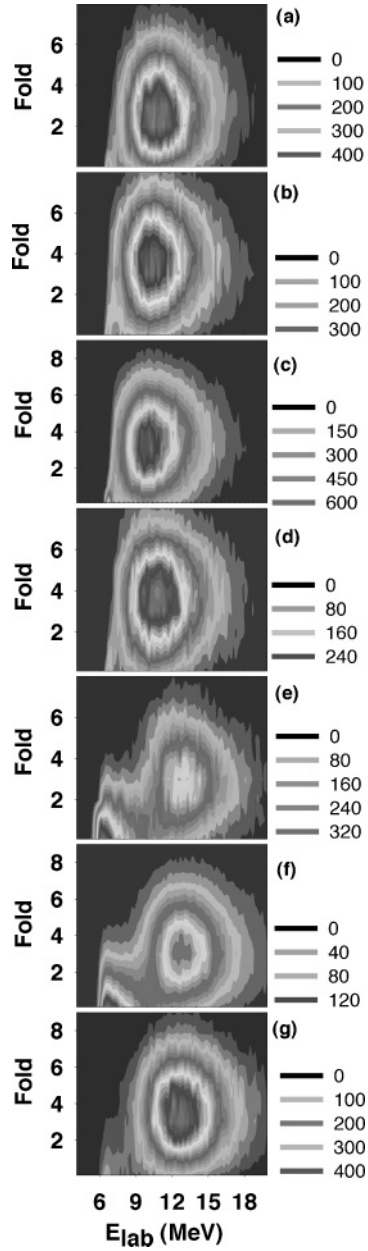

FIG. 1. (a)–(g) Two dimensional plots of γ-ray fold versus α-particle energy (laboratory) measured at $\theta_{lab} = 125^\circ$, for the systems from (a) to (g) see Table I, respectively.

III. DATA ANALYSIS

A. Residue angular momentum and γ-ray multiplicity

The measured fold distributions were analyzed to extract the first two moments of the corresponding γ-ray multiplicity distribution ($\langle M_\gamma \rangle$, $\langle M_\gamma^2 \rangle$) using the procedure given in [14] that

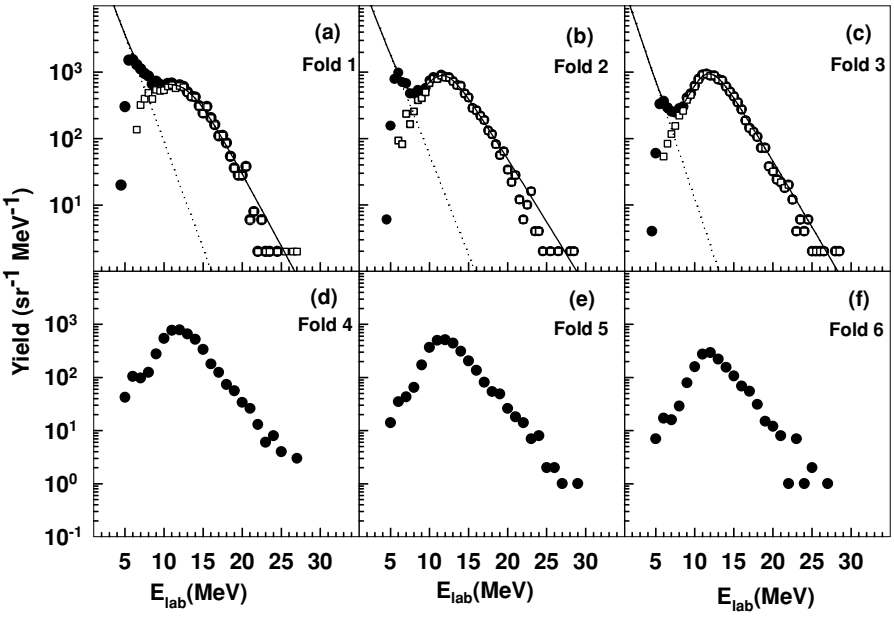

FIG. 2. (a)–(f) Laboratory α-particle energy spectra measured at $\theta_{lab} = 153^\circ$ in $^{11}B + ^{115}In$ reaction for folds 1 to 6 (filled circles). For folds 1 to 3, the solid line is the fit to the spectrum including the low-energy part, the dotted line is the fit to the low-energy background part of the spectrum, and the open squares represent background subtracted spectra. For fold 4 and above, no background subtraction was done because the data above an energy of 15 MeV are essentially free of background (see text).

works well for the present type of low-efficiency multiplicity setup and also used in our earlier work [15]. The conversion procedure from fold to multiplicity was validated by measuring fission γ-ray multiplicity using a ^{252}Cf spontaneous fission source. The average γ-ray multiplicity of ^{252}Cf was found as ~7.8 (9.3 in the second set), which is consistent with the earlier reported values [16–18]. The compound nucleus angular momentum J_{CN} was assumed to be linearly related with residue γ-ray multiplicity M_γ given as

$$J_{CN} = a_m M_\gamma + \delta L_\alpha, \tag{2}$$

where δL_α is the orbital angular momentum carried away (predominantly) by evaporated α particles. Under such an assumption, following relations hold good;

$$a_m = \sqrt{\frac{\langle J_{CN}^2\rangle - \langle J_{CN}\rangle^2}{\langle M_\gamma^2\rangle - \langle M_\gamma\rangle^2}}, \tag{3}$$

and

$$\langle \delta L_\alpha\rangle = \langle J_{CN}\rangle - a_m\langle M_\gamma\rangle. \tag{4}$$

The a_m and $\langle \delta L_\alpha\rangle$ values were determined as given in Table II by using the moments $\langle J_{CN}\rangle$ and $\langle J_{CN}^2\rangle$ obtained from the Bass systematics [19] used in the statistical model code PACE2. The PACE2 code also provides mean values of residual nucleus angular momentum distributions $\langle J_{res}\rangle$ using its trace-back feature and these values are also shown in Table II for each system. It is observed that $\langle \delta L_\alpha\rangle$ determined is of similar magnitude as the difference of $\langle J_{CN}\rangle$ and $\langle J_{res}\rangle$ calculated from PACE2, as one would expect. This establishes consistency in the derived average spin values from the γ-ray-multiplicity measurements.

For the present analysis, it is necessary to assign an average angular momentum for each γ-ray-multiplicity fold. This was done by adopting the following procedure. For each reaction, the residue spin distribution after α-particle emission (J_{res}) was determined using the trace-back feature of PACE2 and this was converted to a corresponding γ-ray-multiplicity distribution M as a row matrix $\mathcal{A}_M$, where the elements are $M^i = J_{res}^i/a_m$, $i = 1, N_m$. Here N_m is decided by J_{res}^{max}, where J_{res}^{max} is the maximum value of residue spin populated. The parameter a_m was chosen to be 1.6 (1.5 for the second set), which is consistent according to the experimentally estimated values as shown in Table II. The fold distribution F for a given value of multiplicity M was calculated with a Monte Carlo technique [20,21] by simulating the history of each γ ray in the cascade. In the calculation for F all the BGO detectors were assumed to be of equal efficiency. If N_D is the number

TABLE II. Moments of experimental γ-ray multiplicity ($\langle M_\gamma\rangle$, $\langle M_\gamma^2\rangle$), compound nuclear angular momentum ($\langle J_{CN}\rangle$, $\langle J_{CN}^2\rangle$), residue spin ($\langle J_{res}\rangle$), and related parameters.

Index	Reaction	$\langle M_\gamma\rangle$	$\langle M_\gamma^2\rangle$	$\langle J_{CN}\rangle(\hbar)$	$\langle J_{CN}^2\rangle(\hbar^2)$	$\langle J_{res}\rangle(\hbar)$	a_m	$\langle \delta L_\alpha\rangle(\hbar)$
a	$^{19}F + ^{93}Nb$	8.8	102.9	19.8	444.5	14.2	1.45	6.9
b	$^{24}Mg + ^{89}Y$	11.3	159.1	25.8	753.2	17.1	1.68	6.8
c	$^{27}Al + ^{89}Y$	10.6	141.0	25.9	759.1	17.5	1.71	7.7
d	$^{24}Mg + ^{93}Nb$	11.4	159.5	26.7	807.2	17.3	1.78	6.4
e	$^{11}B + ^{115}In$	9.6	115.6	20.3	466.2	14.8	1.52	5.7
f	$^{12}C + ^{115}In$	10.6	141.6	23.4	619.5	17.0	1.58	6.6
g	$^{16}O + ^{115}In$	11.6	164.8	24.0	651.3	17.8	1.55	6.0

of BGO detectors, then there are $(N_D + 1)$ number of firing blocks, $B^i (i = 0, N_D)$, that are assumed to be exposed by a cascade of γ rays of length M. One additional block B° is to take into account of the no firing condition. Elements of fold distribution F are $F^i, i = 0, N_D$. In the algorithm, if ith block is fired by any one γ ray of the cascade, then content of B^i is increased by 1 ($\triangle B^i = 1$) for $i = 0, N_D$. If a second γ ray of the same cascade hits the same detector (registered or not), it cannot hit any other detector and hence it should be lost. The rejection of these multiple hitting γ rays is taken into account by looking for the condition that the total increment $\triangle B^i \geqslant 1, i = 1, N_D$. If this condition is satisfied by n number of blocks after the full cascade has fired the BGO setup, then the nth element of the fold distribution F would be increased by 1. To obtain the full fold distribution F, the simulation is repeated typically for 10^6 γ-ray cascades of length M. Finally, to write in terms of probability, each element F^i is divided by 10^6. The calculations were carried out for multiplicity values of $M = 1$ to $M = M_{\max}$, where $M_{\max} = J_{\text{res}}^{\max}/a_m$. By combining all the above calculations, a two-dimensional BGO response matrix (multiplicity vs. fold), $\mathcal{B}_{M,F}$, was obtained. Using the matrices $\mathcal{A}_M$ and $\mathcal{B}_{M,F}$ a weighted BGO response matrix, $\mathcal{C}_{M,F} = \mathcal{A}_M.\mathcal{B}_{M,F}$ was obtained for a specific residue spin distribution. Finally, by projecting the matrix $\mathcal{C}_{M,F}$ on the fold axis, weighted multiplicity distributions for various folds were obtained. The first moment of the spin distribution (average value of angular momentum) for each fold F was calculated as follows:

$$\langle J \rangle = a_m \frac{\sum_{M=1}^{M_{\max}} M.\mathcal{C}_{M,F}}{\sum_{M=1}^{M_{\max}} \mathcal{C}_{M,F}}. \tag{5}$$

In similar fashion the second moment of the distribution $\langle J^2 \rangle$ for each fold was calculated. From here, the width of angular momentum window for each fold was deduced as follows:

$$\delta J = \sqrt{\langle J^2 \rangle - \langle J \rangle^2}. \tag{6}$$

The width δJ is large for lower folds and small for higher folds for each reaction. The uncertainty in the assignment of $\langle J \rangle$ varied from $\pm 5\hbar$ to $\pm 2\hbar$ in going from low folds to high folds.

Figure 3 shows the values of $\langle J \rangle$ and width δJ as a function of γ-ray fold, calculated as above for various systems. It is seen that in going from fold 1 to 8, the angular momentum is spanned in the range of $10\hbar$ to $25\hbar$ for all the systems. The particular nonlinear dependence of $\langle J \rangle$ on fold arises due to a combination of the low efficiency of the BGO setup and the shape of the angular momentum distribution in residual nucleus.

B. Determination of the level-density parameter

The experimental fold-gated α-particle energy spectra were compared with the theoretical spectra. The theoretical spectra were generated using the events file of PACE2 code, by taking into account the efficiency of the BGO detector setup and the angular momentum removal by γ rays, as discussed later in this subsection. The level density $\rho(E_X, J)$ used in the PACE2 calculations above an excitation energy $E_X \sim 5$ MeV is given

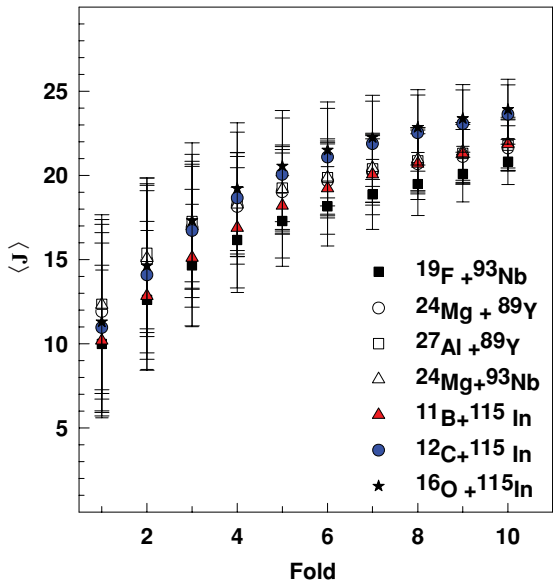

FIG. 3. (Color online) The values of average angular momentum $\langle J \rangle$ (in unit of $\hbar$) derived as a function of γ-ray fold for the various systems. The error bars indicate the width δJ (see text).

by

$$\rho(E_X, J) = \frac{(2J+1)}{12}\sqrt{a}\left(\frac{\hbar^2}{2\Im}\right)^{3/2}\frac{\exp(2\sqrt{aU})}{U_{\text{ex}}^2}, \tag{7}$$

where $U_{\text{ex}} = E_X - \Delta P(Z) - \Delta P(N)$ and $U = U_{\text{ex}} - E_{\text{rot}}$, where $E_{\text{rot}} = \frac{\hbar^2}{2\Im} J(J+1)$ is the rotational energy. $\Delta P(Z)$ and $\Delta P(N)$ are the ground-state pairing energy differences obtained from Gilbert and Cameron's compilation for odd-even mass differences. The moment of inertia $\Im$ was calculated using Sierk rotating liquid drop model [22] and it can be parameterized for the calculation in the spin cut-off parameter as $\sigma^2 = \Im t/\hbar^2$, where t is the thermodynamic temperature. With the spin cut-off parameter, Eq. (7) can be rewritten in the traditional form as in, for example, Refs. [5,23]. We used the following form for level-density parameter a [2], which is widely used in phenomenological descriptions of nuclear level density:

$$a = \tilde{a}\left\{1 - \frac{\triangle S}{U}[1 - \exp(-\gamma U)]\right\}, \tag{8}$$

where $\tilde{a}$ is the asymptotic value of the level-density parameter and γ isthe shell damping factor for which we have used the value 0.054 MeV^{-1}. The shell correction factor $\triangle S$ was calculated using the Swiatecki and Mayer formalism [24], with the convention of being +ve for the closed-shell nuclei. The value of $\tilde{a}$ was externally varied in the code through the input card. At E_X below ~5 MeV, Gilbert and Cameron's constant temperature formula was used for the level density. The γ-ray decay intensities were taken from the RIPL compilation [25]. The initial angular momentum distribution for the compound nucleus was obtained from the Bass systematics [19] for the fusion cross section together with an angular momentum diffuseness of $\sim 0.5\hbar$. The values of target and projectile spins were also provided in the input.

The other important input parameter in the PACE2 calculation is the transmission coefficient as a function of energy and orbital angular momentum of the emitted particle. This is conventionally generated by the optical model potentials (OMP). In the present calculations for α-particle emission, the OMP parameters of Igo and Huizenga [26] were used.

We have thus adopted a widely used set of input parameters for the PACE2 calculations. Our aim in the present work is to compare the shape of the fold-gated as well as gross (summed over all the folds) experimental α-particle spectra with corresponding spectra from PACE2 calculations at well above the evaporation barrier energy and derive the inverse level-density parameter $K = A/\tilde{a}$. By limiting the analysis to the spectral shape at well above evaporation barrier, the uncertainties associated with the barrier transmission coefficients are avoided. The normalization of the shape of the experimental spectra with that predicted using a statistical model calculation was done by matching the area under the predicted spectra in the selected energy interval with that of the experimental spectra in the same energy interval. No attempts were made to fit the multiplicity of α particles. The effect of scaling of yrast line on the level-density parameter was separately investigated as detailed below.

Fold-gated α-particle energy spectra (in the center-of-mass frame) were calculated within the statistical model code PACE2 using Eq. (7) for the E_X and J dependence of nuclear level density. A fitting procedure was adopted for determining K using the following steps. The program was run typically for 10^6 events for the decay of compound nucleus corresponding to each reaction. From the events file, decay chains were traced in the (E_X, J) plane. The distribution of cross section leading to different J and E_X states after emission of α particles was obtained. From this, a 2D matrix $\mathcal{D}_{E_\alpha^{\text{c.m.}}, J_{\text{res}}}$ that corresponds to residue spin distribution for each $E_\alpha^{\text{c.m.}}$ was extracted. The residue spin distribution was then converted to a γ-ray multiplicity distribution using the prescription $M = J_{\text{res}}/a_m$, and thus $\mathcal{D}_{E_\alpha^{\text{c.m.}}, J_{\text{res}}}$ was transformed to another 2D matrix $\mathcal{E}_{E_\alpha^{\text{c.m.}}, M}$ ($E_\alpha^{\text{c.m.}}$ vs. γ-ray multiplicity). The parameter a_m was chosen to be 1.6 (1.5 for the second set) as discussed in Sec. III A. It was seen that by varying the parameter a_m from 1.5 to 1.9, the conclusions obtained from the results were not changed. As discussed in Sec. III A, a BGO response 2D matrix (multiplicity vs. fold), $\mathcal{B}_{M,F}$ was obtained and using these two matrices a cross-section 2D matrix $\mathcal{F}_{E_\alpha^{\text{c.m.}}, F} = \mathcal{E}_{E_\alpha^{\text{c.m.}}, M}.\mathcal{B}_{M,F}$, was determined. Finally, by projecting the cross-section matrix on the energy axis, the α-particle energy spectra for various folds were arrived at. By summing over all fold-gated spectra, the gross spectrum was obtained.

We have used the least-squares method to analyze the data to extract the most probable values and corresponding variance in the parameters being determined. In the present case, the inverse level-density parameter K was varied to fit the energy spectrum. The α-particle energy spectrum is a nonlinear function and, in this case, least-squares solutions are determined by minimizing the statistical variance given by

$$S(K) = \sum_{i=1}^{N} \frac{[Y_i - f(K, E_i)]^2}{\sigma_i^2}, \tag{9}$$

where Y_i is the double differential cross section in ith energy bin, $f(K, E_i)$ is the result of PACE2 calculation for the same energy bin for inverse level-density parameter K after normalization of the spectrum as discussed previously, and σ_i is the statistical error in the measured cross section. The energy region in α-particle spectra to calculate the $S(K)$ value was chosen from 18.5 to 31.5 MeV for all the systems. By definition, the best-fit parameter $\bar{K}$ occurs when $S(K)$ is minimum. If the functional form of $f(K, E)$ is correct and the errors, σ_i, in Y_i are normally distributed, then the minimum $S(\bar{K})$ obey the chi-square $\chi^2(N-1)$ distribution with $N-1$ degree of freedom, where N is the number of data points considered. We have evaluated $S(K)$ as a function of K using the above equation and, in most cases, a parabolic dependence of $S(K)$ on the parameter K was observed. Best-fit parameter $\bar{K}$ was determined from the minimum of the parabola, from which the level-density parameter a can be determined using Eq. (8) with $\tilde{a} = A/\bar{K}$. However, because at an excitation energy around 30 to 40 MeV, the multiplying factor in square bracket in Eq. (8) is nearly unity for all known values of $\triangle S$, we used the approximation $a = \tilde{a}$ for quoting the results. To define error δK on $\bar{K}$, an interval of 68.3% confidence level was determined (corresponding to one standard deviation) using a limit on $S(K)$ defined as [27]

$$S_L = S(\bar{K}) + \frac{S(\bar{K})}{N-1}. \tag{10}$$

The error δK is defined as the intercept of the parabola with the limit value S_L. Using the same technique of least squares, the effect of yrast scaling factor FY was deduced for a selected value of K for the $^{11}\text{B} + ^{115}\text{In}$ reaction as a typical case study.

IV. RESULTS AND DISCUSSION

A. Particle spectra and determination of K.

α-particle evaporation multiplicity ν_α was estimated for the present reactions from the measured evaporation cross sections and Bass fusion cross sections. The values of ν_α calculated using PACE2 code were found to be of similar magnitude and are listed in Table I. As pointed out earlier, α-particle emission leaves residual nuclei with $Z_R = Z_{\text{CN}} - 2$. A major fraction of the α particles is emitted as first chance emission and the remaining will be by and large after one neutron emission. The residual nucleus excitation energy after first chance α-particle emission is given by

$$E_X = E_{\text{ex}}^{\text{CN}} - S_\alpha - E_\alpha^{\text{c.m.}}, \tag{11}$$

where $E_{\text{ex}}^{\text{CN}}$, S_α, and $E_\alpha^{\text{c.m.}}$ are the initial excitation energy of the compound nucleus, α-particle separation energy, and kinetic energy of the emitted α particle, respectively. The approximate range of E_X is between 30 to 40 MeV for α-particle energies selected for the present analysis. The intrinsic excitation energy available for the residual nuclei will be, however, less than E_X by energy locked in the rotational energy of the nuclei, E_{rot}. An estimate of the E_{rot} was made for different angular-momentum values using RLDM moment of inertia. Accordingly, in this mass region and for $J = 20\hbar$, the value of E_{rot} is 4.4 MeV. Similarly the change in rotational energy in

going from $J = 10\hbar$ to $20\hbar$ in ^{122}Te is only 3 MeV. From the above discussion, it can be seen that the net excitation energy of the residual nucleus after α-particle emission is still in a broad range of energies between 30 to 40 MeV and the residue mass has a small broadening of one or two units. There is no broadening in residue charge due to nonselection of the exit channel.

Using the least-squares method, the experimental gross spectra were analyzed by comparing with PACE2 predictions. As mentioned earlier, the calculated α-particle yields at the selected high-energy region were normalized to the experimental yields while fitting the spectra. The open circles and solid histograms shown in Fig. 4 are experimental and PACE2 calculated gross spectra, respectively, after the normalization.

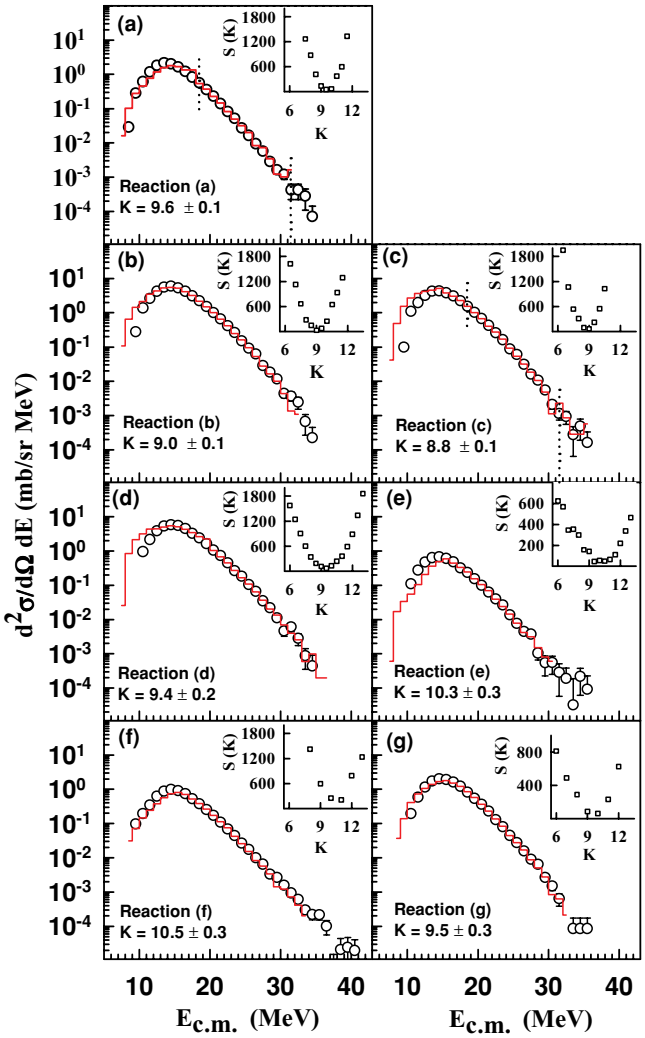

FIG. 4. (Color online) (a)–(g) Gross α-particle energy spectra in the center-of-mass system (open circles) in reactions from (a) to (g) Table I and the results of PACE2 statistical model calculation (solid histograms). The vertical dotted lines in the top panels show the extremes of the energy interval chosen for the fits and this interval was same for all the fits. The reaction index and the K value obtained (with error bar) are shown at the bottom of each panel. In the inset, statistical variance $S(K)$ is shown as a function of K from where the best fit K value was determined as discussed in the text.

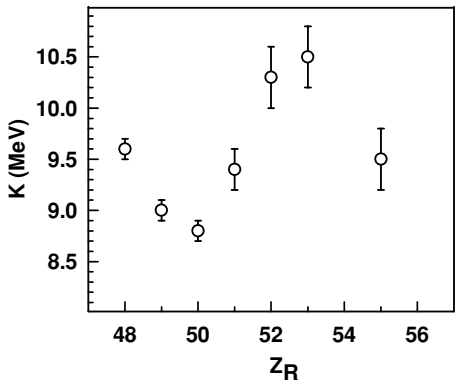

FIG. 5. Inverse level-density parameter K determined from the gross spectra, shown as a function of Z of the residual nuclei.

The vertical dotted lines in the top panels show the extremes of the energy interval chosen for the fits, and this interval is same for all the fits. The insets in the panels show the nearly parabolic variation of $S(K)$ with the parameter K. The minimum of the parabola corresponds to the best fit value of the inverse level-density parameter K. The best fit K values for all the systems are given in Table I. Figure 5 shows the variation of K as a function of Z of the residual nuclei (Z_R). The "gross" K values for nuclei studied in the present work lie in the range of 9.0 to 10.5 and are within the liquid-drop-model estimates [2] for $Z \sim 50$ region. In an earlier work [12,28], the "gross" K values for $Z_R = 48$ and 52 were measured in the same excitation energy region. The earlier results had errors of ± 1 unit and may be considered to be consistent with the present measurement within error bars. The data given in Fig. 5 show that the value of K is strictly not same for all the systems studied. The average excitation energy of the residual nuclei after α-particle emission is around 35 MeV for the present systems, which according to Ref. [2] is above the energy required for washing out of shell effects. It is seen from Fig. 5 that the value of K is the lowest for $Z_R = 50$, in contrast with what one might have expected from known behavior of shell effects, by assuming persistence of shell effects even at this excitation energy. Maximum value for K is observed for $Z_R = 52$ and 53. We have no microscopic understanding of these observations but would like to point out that similar differences in level-density parameter in neighboring nuclei with excitation energy around 60 to 90 MeV have been observed [29]. To understand the role of dinuclear complex formation during fusion process in producing these apparent differences, we have calculated the Businaro-Gallone critical mass asymmetry for various ℓ-partial waves in present systems. The effect of entrance-channel mass asymmetry in compound nucleus formation has been studied earlier in terms of the mass-asymmetry parameter α with respect to $\alpha_{\rm BG}$ (Businaro-Gallone critical mass asymmetry) [30]. Figure 6 shows the variation of $\alpha_{\rm BG}$ as a function of angular momentum for all the systems studied in the present work. It is seen that for all the systems studied, the mass-asymmetry parameter α is on the same side of the $\alpha_{\rm BG}$ line for all angular momentum values (i.e., $\alpha > \alpha_{\rm BG}$ for all J). Therefore, the entrance-channel effect with respect

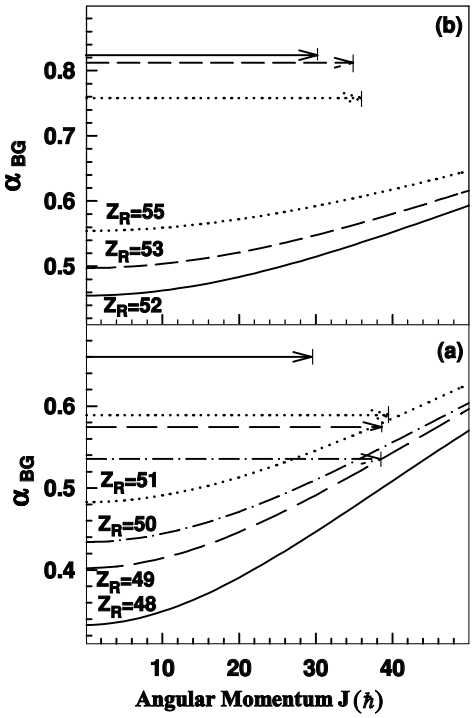

FIG. 6. α_{BG} as a function of entrance-channel angular momentum J, for systems from a to d [panel (a)] and for systems e to g [panel (b)]. In the figure, the arrows on the y axis indicate the position of mass-asymmetry parameter, α, for different target-projectile systems that terminate at the corresponding l_{graz} see Table I. The pattern of the arrow is same as for the corresponding line for α_{BG}. Corresponding to each reaction the value of Z_R is shown along each line.

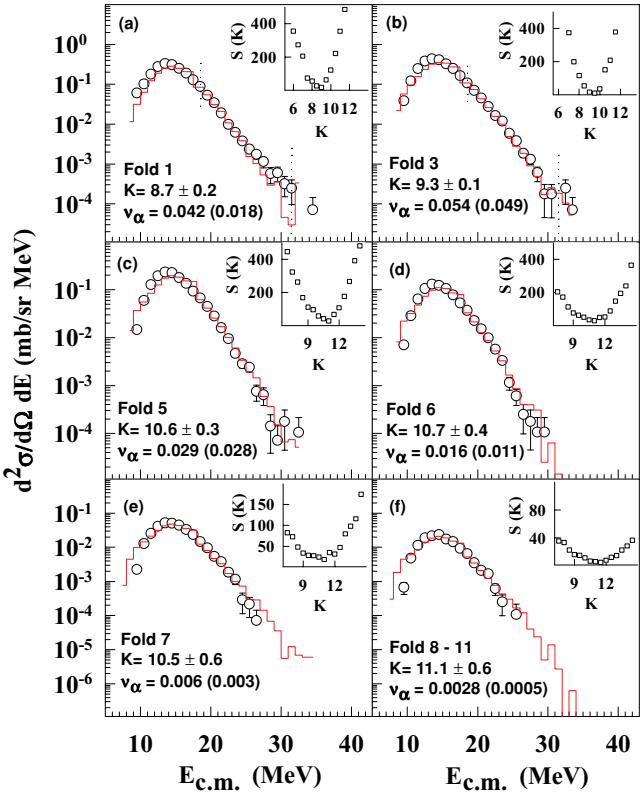

FIG. 7. (Color online) (a)–(f) Fold-gated α-particle energy spectra in a center-of-mass system for $^{19}F + ^{93}Nb$ reaction for various folds (open circles) along with the results of PACE2 statistical model calculation (solid histograms). The vertical dotted lines in the top panels show the extremes of energy interval chosen for the fits and this interval was same for all the fits. The fold number, the K value obtained (with error bar), and experimental as well as calculated (in the parenthesis) multiplicity of α particles, ν_α, are shown at the bottom of each panel. In the inset, statistical variance is shown (open squares) as a function of K from where the best-fit K value was determined as discussed in the text.

to BG point is not expected to play a role for the present systems and all the systems are expected to undergo normal compound nuclear formation without a dinuclear complex formation. In the work by Liang *et al*. [31] light charged particle emissions from ^{156}Er compound nucleus, populated by $^{12}C + ^{144}Sm$ and $^{60}Ni + ^{96}Zr$ reactions at same excitation energy, were measured in coincidence with the evaporation residues. The high-energy slope of light charged particle spectra for ^{60}Ni-induced reaction was found to be steeper than for the ^{12}C-induced reaction. Similar observation was reported by Govil *et al*. [32] for other systems. However, in these earlier studies, the systems correspond to a large difference in the entrance channel mass asymmetry, which lies on the opposite side of α_{BG}.

B. Angular momentum dependence of K

Figures 7–13 show the measured α-particle energy spectra for all the systems for various folds (open circles) and the corresponding PACE2 best fits (solid histograms) using the same procedure as described earlier. The fold number, the K value obtained (with error bar), and experimental as well as calculated (in the parenthesis) multiplicity of α particles, ν_α, are shown at the bottom of each panel. In the insets, the results of the least-squares analysis are shown. It is seen that for all cases, a well-defined minimum in $S(K)$ is obtained as a function of K. The values of K corresponding to the minima were taken as the best-fit values. Figure 14 shows the variation of K with γ-ray fold for all the systems.

The Z_R values are shown beside each plot. A more physical understanding of the behavior of inverse level-density parameter K as a function of angular momentum may be achieved by plotting the variation of K with $\langle J \rangle$. The fold to angular momentum conversion was carried out using the calculations presented in Fig. 3. In Fig. 14 and Fig. 15 we also show the "gross" value of K (average $\pm\delta K$) as a band for comparison. The overall trend does not suggest a constant value for K over the full angular momentum range for all the systems. Some general observations can be made from Fig. 15 regarding the angular-momentum dependence of K for nuclei of different charge Z_R. It is seen that for $Z_R = 49$, 50, and 51 corresponding to the shell region, there is a flat behavior for low angular momentum and the results agree with "gross" K value. However, a downward trend is observed for higher J values. Once the shell region is crossed, for $Z_R = 52$ and 53 a dramatic

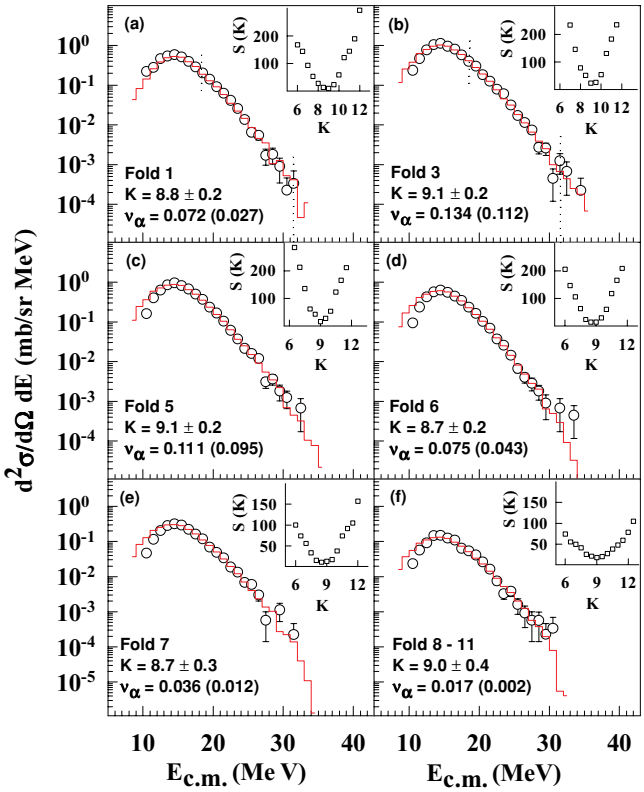

FIG. 8. (Color online) Same as in Fig. 7 but for the $^{24}Mg + ^{89}Y$ reaction.

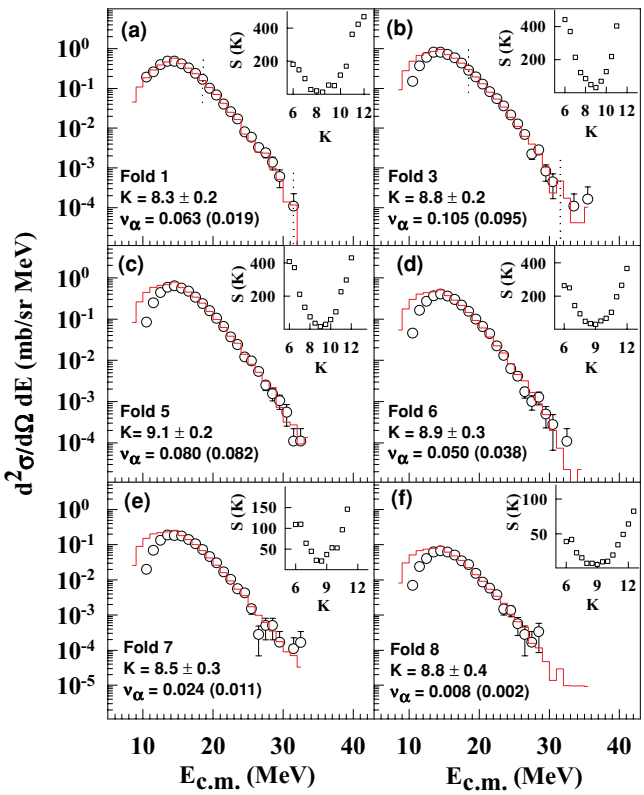

FIG. 9. (Color online) Same as in Fig. 7 but for the $^{27}Al + ^{89}Y$ reaction.

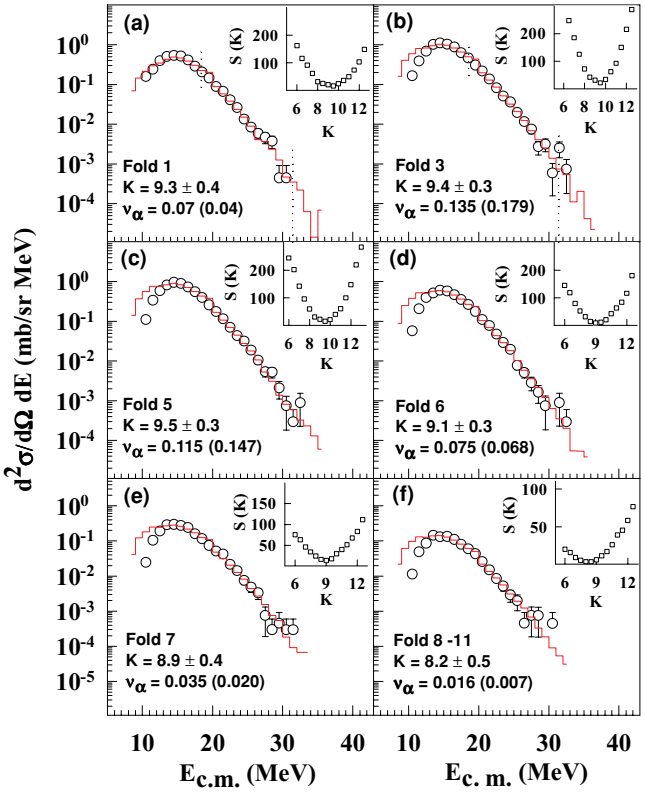

FIG. 10. (Color online) Same as in Fig. 7 but for the $^{24}Mg + ^{93}Nb$ reaction.

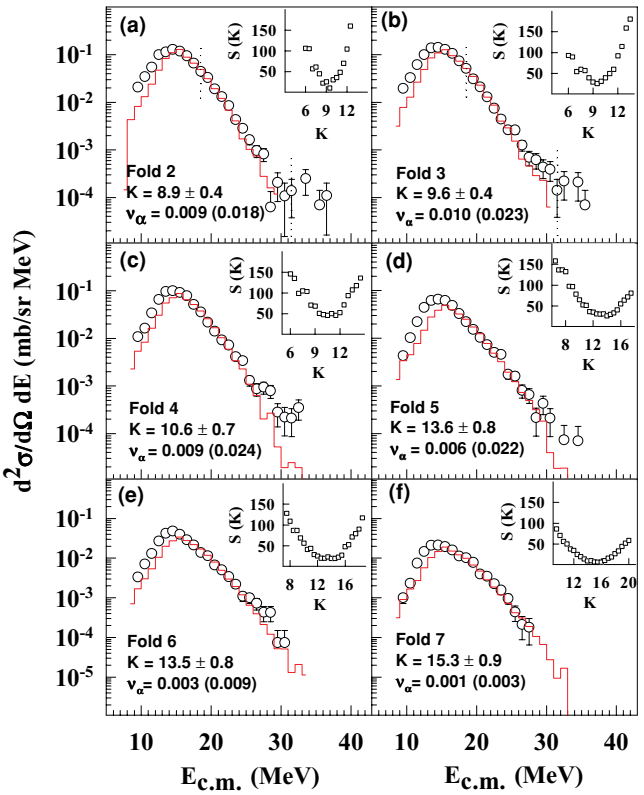

FIG. 11. (Color online) Same as in Fig. 7 but for the $^{11}B + ^{115}In$ reaction.

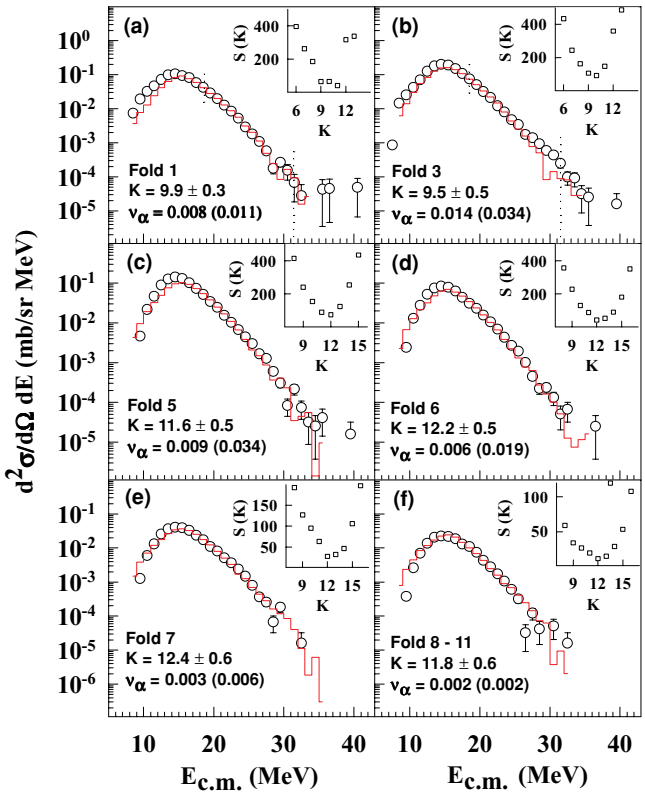

FIG. 12. (Color online) Same as in Fig. 7 but for the $^{12}C + ^{115}In$ reaction.

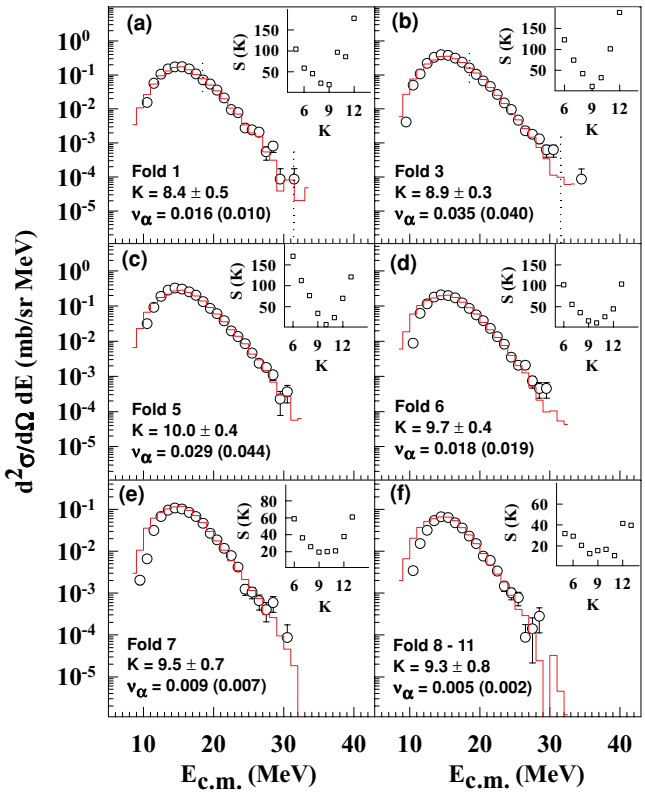

FIG. 13. (Color online) Same as in Fig. 7 but for the $^{16}O + ^{115}In$ reaction.

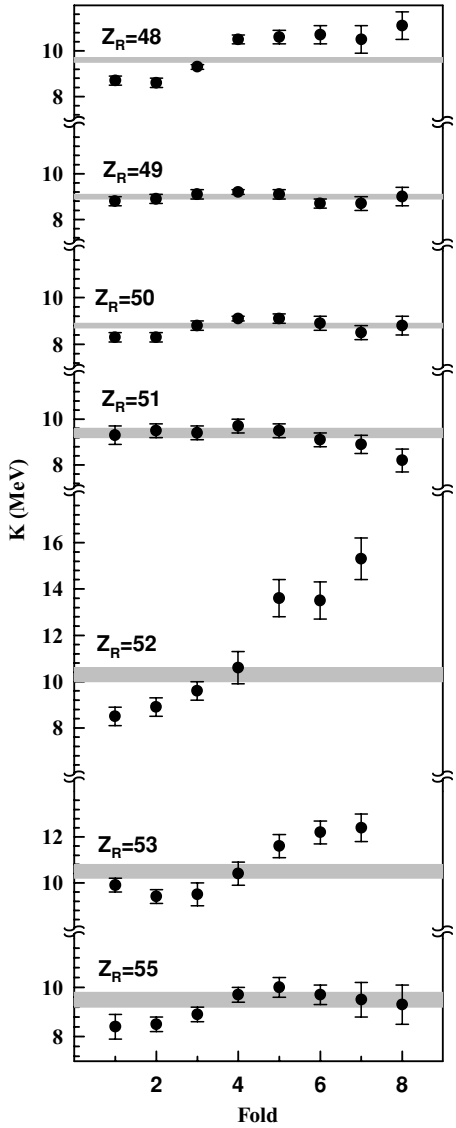

FIG. 14. Inverse level-density parameter K as a function of the γ-ray fold for different Z_R. The shaded band in each panel correspond to "gross" K value.

change in the trend can be observed. In a repeat measurement we have reconfirmed the behavior for the $Z_R = 52$ system where there is a strong increase in K with angular momentum. For this system, the K values are lower than the "gross" K value in the low-angular-momentum region and are larger for higher values of angular momentum. This trend is continued for $Z_R = 53$ and 48 as well but in a diminished manner. For $Z_R = 55$ the trend is also similar but with a much weaker variation of K with angular momentum.

To explain the slope of the experimental α-particle energy spectra in the high-energy region, one can alternately vary the yrast scaling factor FY by fixing K to a constant value. This was tried out for the $Z_R = 52$ system by fixing K at 9.0 and increasing the yrast scaling factor FY to $\sim$2.5 for high folds. From the least-squares fits, it was observed that if K is fixed, the factor FY required to fit the fold-gated spectra for the $Z_R = 52$ system increases as residue angular

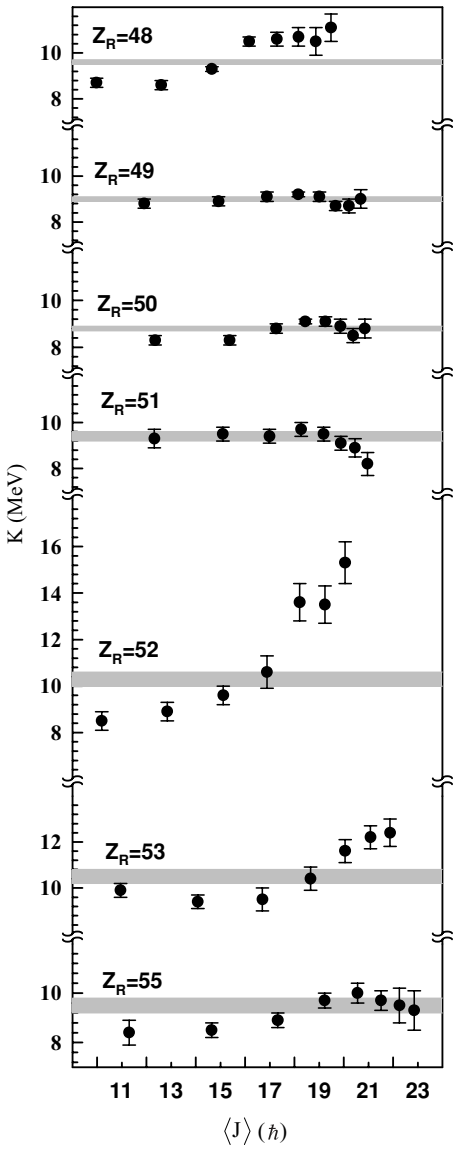

FIG. 15. Inverse level-density parameter K as a function of $\langle J \rangle$ for different Z_R. The shaded band in each panel correspond to "gross" K value.

momentum or the fold number increases. Increase of FY at high spin implies increase of rotational energy from RLDM value at higher spin and this is possible if moment of inertia of the nucleus is reduced from the RLDM value at high spin. The present results are the first of their kind as far as we know. The observation of significant variations in K over and above the "shell corrected" level-density parameter is not fully explained. There are no theoretical calculations available for a direct comparison with the present results.

In our analysis for the inverse level-density parameter K, we relied on Bethe's Fermi-gas formula for the level densities [Eq. (7)]. The spin cut-off parameter for angular-momentum distribution of levels was included in the formula. A recent theoretical analysis of excitation energy and angular-momentum dependence of level densities using microscopic SPA + RPA approach [33] showed that in mid-mass nuclei the spin cut-off approximation in Bethe's formula works well for $J \leqslant 35\hbar$ at excitation energy $E_X = 30$ MeV. It was found that with an appropriate E_X-dependent value of spin cut-off parameter, Bethe's formula almost reproduces SPA and SPA + RPA results at different excitation energies below a certain J value. Because the residual nucleus excitation energies of interest in the present work are around ∼35 MeV and angular-momentum values are below $35\hbar$, it may be stated that Bethe's formula adequately accounts for the angular-momentum distribution of the levels. The correspondence between the values of K used in Bethe's formula and values of K calculated using SPA was discussed in Ref. [34] for various temperature and angular momentum domains. According to Ref. [34], instead of a full SPA calculation for the level density, it should be enough to use Bethe's formula with K calculated using SPA. Similarly, the experimentally determined K values using the Bethe's formula in a statistical model code should show correspondence with K values calculated using the SPA [12]. It would be interesting to obtain microscopic calculations of K for various angular-momentum domains and compare with the present results.

The authors of Ref. [6] pointed out they are the first ones to calculate the level-density parameter $a(E)$ and the spin cut-off parameter for a large number of nuclei using a realistic microscopic approach. The calculations were carried out at excitation energies of neutron resonance reactions. As expected from their microscopic theory, the spin cut-off parameter showed structures that reflect the angular momentum of the shell-model orbitals near the Fermi energy. The results from the present experiment will provide a testing ground for the microscopic model calculations at moderate excitation energies and angular momenta.

It may be noted that the strong angular-momentum dependence is seen dominently for the $^{11}B + ^{115}In$ system, which is a highly asymmetric system as compared to other systems. It would be pertinent to verify if a less asymmetric beam-target combination producing same compound nucleus also displays the above strong dependence of K on angular momentum. The number of target-projectile combinations leading to same compound system for $Z_R = 52$ is limited. However, it would be of interest to carry out further measurements with systems of ranging entrance-channel mass asymmetry in this Z region to rule out the mass-asymmetry effect on the value of K.

V. SUMMARY

In the present work, we have measured the gross as well as γ-ray-multiplicity fold-gated α-particle energy spectra in reactions that populate residual nuclei in the $Z \sim 50$ region with an excitation energy range from 30 to 40 MeV. In the analysis, each γ-ray multiplicity fold was assigned a corresponding average angular momentum in the residual nuclei following a procedure that utilizes the decay simulations and detector efficiency factors. Gross as well as fold-gated α-particle energy spectra were least-squares fitted with the statistical model code PACE2 to determine the inverse level-density parameter $K = A/a$. The "gross" K values are seen to be in the

range 9.0–10.5 and are within liquid-drop-model estimates for the systems in this Z region. The inverse level-density parameters K as a function of angular momentum determined from the present study showed several interesting features, not accounted by the shell- and angular-momentum-corrected values of K used in PACE2 calculation. These results point out to certain effects not accounted for in the above prescriptions and may provide opportunity to test the microscopic model calculations.

ACKNOWLEDGMENTS

Authors thank the operating staff of Pelletron accelerator facility for the excellent operation of the machine, D. R. Chakrabarty, Suresh Kumar, R. G. Thomas, P. K. Sahu, R. P. Vind, and Megha Bhike for their help during the experiment. We also thank A. Mitra, A. K. Mohanty, A. Chatterjee, S. Kailas, V. S. Ramamurthy, and S. S. Kapoor for fruitful discussions.

[1] A. Gilbert and A. G. W. Cameron, Can. J. Phys. **43**, 1446 (1965).
[2] A. V. Ignatyuk, G. N. Smirenkin, and A. S. Tishin, Sov. J. Phys. **21**, 255 (1975).
[3] S. K. Kataria, V. S. Ramamurthy, and S. S. Kapoor, Phys. Rev. C **18**, 549 (1978).
[4] Y. Alhassid, G. F. Bertsch, L. Fang, and S. Liu, Phys. Rev. C **72**, 064326 (2005).
[5] K. Kaneko and A. Schiller, Phys. Rev. C **75**, 044304 (2007), and references therein.
[6] M. Gholami, M. Kildir, and A. N. Behkami, Phys. Rev. C **75**, 044308 (2007).
[7] S. Henss, A. Ruckelshausen, R. D. Fischer, W. Kuhn, V. Metag, R. Novotny, R. V. F. Janssens, T. L. Khoo, D. Habs, D. Schwalm, D. Freeman, G. Duchene, B. Haas, F. Haas, S. Hlavac, and R. S. Simon, Phys. Rev. Lett. **60**, 11 (1988).
[8] S. F. Mughabghab and C. Dunford, Phys. Rev. Lett. **81**, 4083 (1998).
[9] J. L. Egido, L. M. Robledo, and V. Martin, Phys. Rev. Lett. **85**, 26 (2000).
[10] A. V. Voinov, S. M. Grimes, C. R. Brune, M. J. Hornish, T. N. Massey, and A. Salas, Phys. Rev. C **76**, 044602 (2007).
[11] A. Gavron, Phys. Rev. C **21**, 230 (1980).
[12] B. John, R. K. Choudhury, B. K. Nayak, A. Saxena, and D. C. Biswas, Phys. Rev. C **63**, 054301 (2001).
[13] H. Ho and P. L. Gonthier, Nucl. Instrum. Methods **190**, 75 (1981).
[14] S. Y. V. D. Werf, Nucl. Instrum. Methods **153**, 221 (1978).
[15] B. K. Nayak, R. K. Choudhury, L. M. Pant, D. M. Nadkarni, and S. S. Kapoor, Phys. Rev. C **52**, 3081 (1995).
[16] R. Varma, G. K. Mehta, R. K. Choudhury, S. S. Kapoor, B. K. Nayak, and V. S. Ramamurthy, Phys. Rev. C **43**, 1850 (1991).
[17] V. V. Verbinski, H. Weber, and R. E. Sund, Phys. Rev. C **7**, 1173 (1973).
[18] D. C. Biswas, R. K. Choudhury, M. Cinausero, B. Fornal, D. V. Shetty, G. Viesti, D. Fabris, E. Fioretto, M. Lunardon, G. Nebbia *et al*., Eur. Phys. J. A **7**, 189 (2000).
[19] R. Bass, Phys. Rev. Lett. **39**, 265 (1977).
[20] A. Mitra, D. R. Chakrabarty, V. M. Datar, S. Kumar, E. T. Mirgule, H. H. Oza, V. Nanal, and R. G. Pillay, Nucl. Phys. **A765**, 277 (2006).
[21] A. Mitra, D. R. Chakrabarty, V. M. Datar, S. Kumar, E. T. Mirgule, and H. H. Oza, Nucl. Phys. **A707**, 343 (2002).
[22] A. J. Sierk, Phys. Rev. C **33**, 2039 (1986).
[23] S. Komarov, R. J. Charity, C. J. Chiara, W. Reviol, D. G. Sarantites, L. G. Sobotka, A. L. Caraley, M. P. Carpenter, and D. Seweryniak, Phys. Rev. C **75**, 064611 (2007).
[24] P. Moller, J. R. Nix, W. D. Myers, and W. J. Swiatecki, At. Data Nucl. Data Tables **59**, 185 (1995).
[25] International Atomic Energy Agency, *Handbook for Calculations of Nuclear Reaction Data: Reference Input Parameter Library, RIPL-2*, Vienna, 2005; http://www-nds.iaea.org/RIPL-2, IAEA-Tecdoc-1506.
[26] J. R. Huizenga and G. Igo, Nucl. Phys. **29**, 462 (1962).
[27] D. Cline and P. M. S. Lesser, Nucl. Instrum. Methods **82**, 291 (1970).
[28] B. John, S. K. Kataria, B. S. Tomar, A. Goswami, G. K. Gubbi, and S. B. Manohar, Phys. Rev. C **56**, 2582 (1997).
[29] J. L. Wile, S. S. Datta, W. U. Schroder, J. Toke, D. Pade, S. P. Baldwin, J. R. Huizenga, B. M. Quednau, R. T. deSouza, and B. M. Szabo, Phys. Rev. C **47**, 2135 (1993).
[30] M. Abe, KEK Report No. 86-26, KEK TH-128, 1986.
[31] J. F. Liang, J. D. Bierman, M. P. Kelly, A. A. Sonzogni, R. Vandenbosch, and J. P. S. van Schagen, Phys. Rev. Lett. **78**, 3074 (1997).
[32] I. M. Govil, R. Singh, A. Kumar, J. Kaur, A. K. Sinha, N. Madhavan, D. O. Kataria, P. Sugathan, S. K. Kataria, K. Kumar *et al*., Phys. Rev. C **57**, 1269 (1998).
[33] B. K. Agrawal and A. Ansari, Nucl. Phys. **A640**, 362 (1998).
[34] B. K. Agrawal and A. Ansari, Phys. Lett. **B339**, 7 (1994).